HUNGARIAN UNIVERSITY OF AGRICULTURE AND LIFE SCIENCES

The effect of 3D printing structures and surfaces on the tribological behaviour of polymer and polymer composites

PhD Thesis

by

Muammel M. Hanon Sharba

DOI: 10.54598/002100

Gödöllő
2022

Doctoral school

Denomination: Doctoral School of Mechanical Engineering

Science: Mechanical Engineering

Leader: Prof. Dr. Gábor Kalácska, DSc
Institute of Technology
Hungarian University of Agriculture and Life Sciences,
Szent István Campus, Gödöllő, Hungary

Supervisor: Dr. László Zsidai, PhD
Institute of Technology
Hungarian University of Agriculture and Life Sciences,
Szent István Campus, Gödöllő, Hungary

…… ……
Affirmation of supervisor Affirmation of head of school

CONTENTS

1. INTRODUCTION, OBJECTIVES

1.1. Introduction

Additive Manufacturing, often known as 3D printing, has drew the interests of industry, academics and research societies, and hobbyists alike. The application of additive manufacturing technologies in several sectors has risen dramatically in recent years. Tribology is the branch of knowledge and technology of surfaces in contact and at a relative motion, in addition to supporting activities aimed at lowering friction and wear-related expenses. Polymer components have been popular in tribological applications for decades, owing to their favourable qualities such as vibration damping capabilities, self-lubrication, and corrosion resistance. Many process parameters can be controlled when producing 3D-printed part structures. The influence of process parameter settings on the mechanical qualities have been described in thorough for various production scenarios.

In the present study, the tribological and mechanical properties of 3D-printed polymers and polymer composites will be determined. This research will lead to better control and optimization of the 3D printing parameters of polymers and will provide a better understanding of the tribological properties of the polymeric elements. These findings will be helpful for the industry, which now started to use the up-to-date additive manufacturing technologies not just for rapid prototyping but also for any products of sliding elements.

1.2. Objectives

Fused deposition modelling (FDM) and digital light projection (DLP) 3D printing techniques will be employed to print specimens using various materials and different manufacturing pross parameters. The produced samples, with this variety of conditions, will be subject to tribological, microstructure, surface roughness and energy, tensile, and hardness tests. The main objectives of the present work are to investigate the following:

a) What is the influence of 3D printing conditions on the intrinsic mechanical, physical, and chemical polymer properties and polymer structure?
b) Comparison of friction and wear behaviour of the different printed polymers in connection with printing options, methods and mechanical properties.
c) Determination of optimal operating conditions of the selected polymers and printing methods.
d) What are the tribo-physical reactions taking place within the sliding interface?
e) Evaluation of the effect of filler/additives attendance in the case of composites.

2. MATERIALS AND METHODS

This chapter presents the materials, equipment, procedures, and processes employed in the current research.

2.1. Design of experiment

In this study, two different 3D printing techniques have been utilized which are FDM and DLP. Thermoplastics in a form of filament are printed by FDM, while DLP uses thermosetting (resin) for producing the parts. For each 3D printing method, two types of materials were examined either neat (pure) or composite polymer. Each individual material was employed to fabricate the required specimens with different print parameters for various tests. These specimens were subjected mainly to tribological and mechanical testing. However, investigating the hardness, surface roughness, surface energy, and morphological characteristics was an inevitable task.

2.2. Determination of tribological properties

A cylinder-on-plate tribometer with a reciprocating motion was used to assess the wear and friction characteristics of the 3D-printed parts. This model system ensures the creation of high surface pressure even at small dimensions (line contact). However, the alternating sliding means both static (at reversal points) and dynamic (at intermediate slides) friction can be measured side by side due to the two-way sliding friction. This allows the stick-slip tendency to be explored by jointly measuring adhesions and slips. The schematic of the cylinder-on-plate apparatus is shown in Fig. 1a.

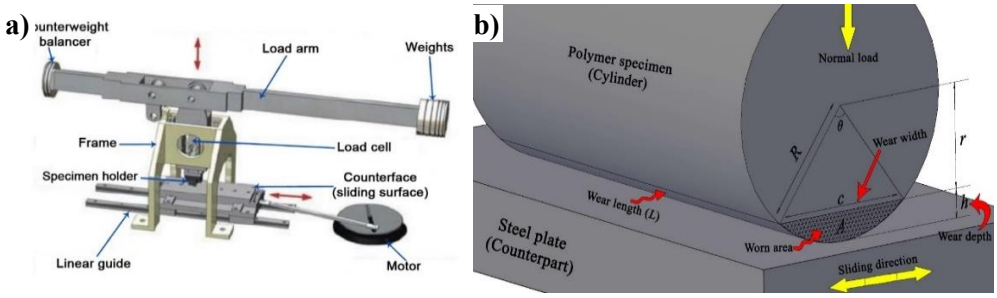

Fig. 1. Schematic of a) cylinder-on-plate tribometer, b) contact of the frictional couple

Table 1. The performed parameters during the tribological tests

Parameter	Value
Surface roughness of steel counterpart, R_a	0.10 – 0.12 μm
Load, F	150-200 N
Alternating motion frequency, f	4.583 Hz
Stroke length	6 mm
Relative humidity, Rh	45 – 50 %
Ambient temperature, T	23 – 25 °C
Test duration, t	60 min

The parameters implemented during the tribological tests are presented in Table 1. Three parallel tests were conducted for each condition to assess the average result. The tribology test begins when the cylindrical shape 3D-printed pieces slide against the tribometer's counterpart. The cylindrical polymer test piece was fixed by means of the sample holder. A schematic diagram for the contact of the frictional couple (the specimen and the counterpart) is shown in Fig. 1b.

2.3. Tensile testing

The FDM 3D-printed test pieces were produced with dimensions of 150 mm by 20 mm by 4 mm according to the dog-bone tensile test geometry of the ISO 527-2: 2012 standard type 1B sample. However, due to insufficiency in the printing dimensions, the DLP printed tensile test pieces were modelled following ISO 527-2, type 1BA, with an overall dimension of 75 mm × 10 mm × 2 mm.

2.4. Microstructure, hardness, surface roughness, and surface energy

A ZEISS brand optical microscope equipped with a mobile stand-alone colour camera type ZEISS Axiocam ERc 5s was used to examine the surface morphology of the printed samples before and after the tribology test. Furthermore, in the case of graphene/resin composite material, the surface morphology was examined using an EVO 40 scanning electron microscope at 20 kV acceleration voltage.

The hardness of the printed test pieces was examined using a shore D hardness device measuring between 0 and 100HD. The penetration is carried out when a steel needle (indenter) is pressed into the testing material and the amount of resistance is displayed at the scale. This indenter needle is a conical point shape with a top cone angle of 35° and a tip radius of 0.1 mm.

A Mitutoyo portable surface roughness tester type SJ-41 connected to a computer was used to measure the surface roughness for tribology specimens prior to and after the tests. A scan length of 5 mm and a cut-off of 0.8 mm were used as test conditions to obtain 2D surface roughness (R_a) measurements as well as the primary profile. The surface roughness was evaluated for all tribology specimens prior to and after the tests.

The drop shape analyser DSA30 was used to measure the contact angle and to determine the surface free energy employing two models (EoS and Fowkes). In the form of droplets, liquids (High-purity distilled water, diiodomethane (CH_2I_2) and cyclohexane (C_6H_{12})) were used to determine the dispersive (γ^D) and polar (γ^P) components of the surface energy. By summing the surface tension components, the value of the total surface energy (γ) was determined

$$\gamma = \gamma^D + \gamma^P. \quad (1)$$

3. RESULTS AND DISCUSSION

The experiment results are presented in this chapter, as well as discussions suggesting the new findings.

3.1. Investigation of tribological properties

3.1.1. Tribology of neat PLA material FDM 3D-printed

The averaged values of the dynamic friction coefficient for all specimens (three print orientation, three colours, and two applied load) were calculated and presented in Fig. 2a. In all conditions, the white polymer exhibited the highest friction, while the grey colour samples offered the lowest friction except in the case of Horizontal under 200 N load. For 150 N applied load (under lower load), the colour has no significant effect on the Horizontal orientation's friction. However, in the 45° angle and the Vertical, the colour showed notable influence. Concerning the 200 N applied load (under higher load), the colour has affected the test pieces' friction in all orientations.

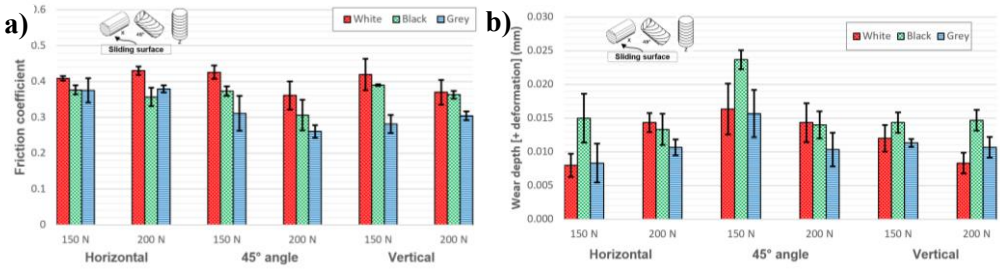

Fig. 2. Comparison of a) dynamic friction coefficient, and b) wear depth

Fig. 2b shows a comparison of the average wear depth obtained during the tribology test. The different colours of PLA polymer also showed somewhat an effect on the wear depth. Mainly, the black coloured specimens reported a high wear depth. In contrast, the white and grey test pieces in most cases were within the same moderate range. There is no certain interpretation in literature about why the wear depth of black colour has increased higher than other colour samples. But the author believes that due to the sliding with the counterpart, the frictional heat boosts the temperature of the specimen's surface. Hence, the black colour samples may subject to the black body features where maximum heat retains in the test piece's body. This was proved through some heat-conductive tests were carried out on the same examined tribology specimens. The black kept the heat for a longer time, indicating the formation of higher temperatures and therefore determining the tribological behaviour.

3.1.2. Tribology of bronze/PLA composite FDM 3D-printed

After evaluating the tribology test data results, the static and dynamic friction coefficient has been obtained (see Fig. 3a). Considering both loads (150 N and

200 N) results, it can be seen that Horizontal and 45° angle have the least dynamic friction coefficient, whereas the Vertical offered the highest friction coefficient values. This can be expounded due to the layers' structure, which is in contact with the sliding surface. However, it can be noticed a bigger difference between the dynamic and static friction coefficients under the load 150 N. What means that sliding under lower loads, increase the tendency for occurring stick-slip phenomenon. As it was possible to hear higher noise while testing Vertical specimens, which indicates the happening of this phenomenon as well. Bearing in mind that under the higher load (200 N), these differences decreased. Therefore, the instability of the sliding also decreases.

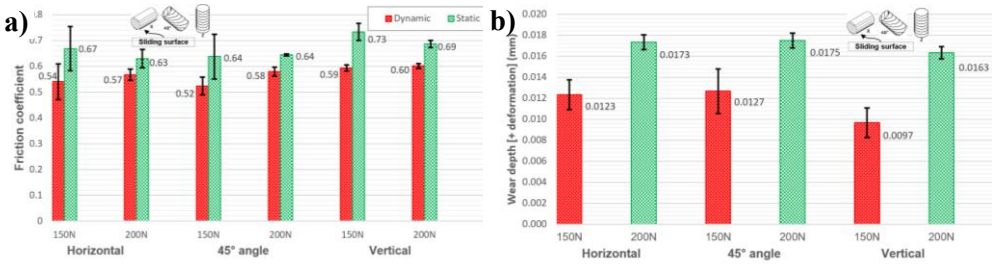

Fig. 3. Comparison of a) static-dynamic friction coefficient, and b) wear depth

Comparison of the average wear depth that occurred during the tribology test is displayed in Fig. 3b. The test pieces exhibited similar behaviour in all orientations against each applied load (150 and 200 N). At the lower load, less wear was observed. Certainly, the lower wear rate specimens are preferable for many implementations.

3.1.3. Tribology of neat resin material DLP 3D-printed

As shown in Fig. 4a, the dynamic friction coefficient obtained from the post-curing process specimens exhibited no significant difference (between 0.72-0.79) among the samples of various print orientations. Nevertheless, the tendency for occurring stick-slip phenomenon has notably increased where the static friction coefficient reached very high values. In contrast, relatively reduced values were observed in the friction coefficient (whether static or dynamic) of the non-cured specimens for all build orientations.

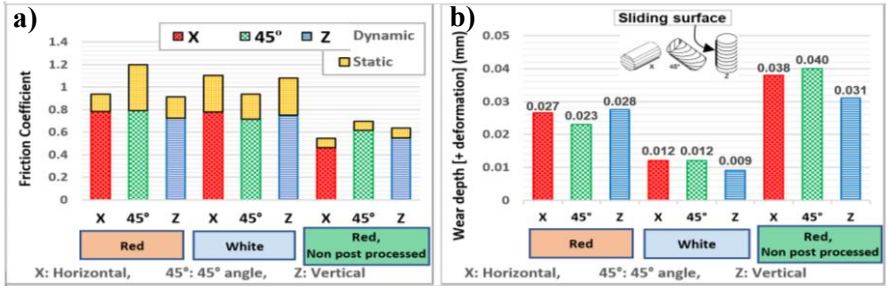

Fig. 4. Comparison of a) friction coefficient, and b) wear depth

Comparison of the wear depth among the tested prototypes in terms of print orientation and the post-curing process is displayed in Fig. 4b. The non-cured specimens demonstrated the highest wear depth as compared to the post-curing test pieces. This indicates the impact of the post-curing process on the hardness (increased) of the surface, that gave the cured specimens better wear resistance.

3.1.4. Tribology of graphene/resin composite DLP 3D-printed

Comparison of the profiles of friction coefficient during tribology tests under a load of 150 N is presented in Fig. 5. Generally, the friction coefficient profile curves go through three stages called running-in, fluctuation, and stable friction. The curves show a sharp increase in the running-in stage because of the static friction behaviour. This stage terminated almost by the end of the first ten meters of the sliding distance in all curves. The length of the fluctuation stage differed for different curves as some of them lasted up to 40 m of sliding distance. The curves obtained show that most of the neat resin test pieces reported an elevated dynamic coefficient of friction ranging from 0.6 to 0.7 in the stable stage. However, the addition of graphene significantly impacted the attitude of the friction coefficient.

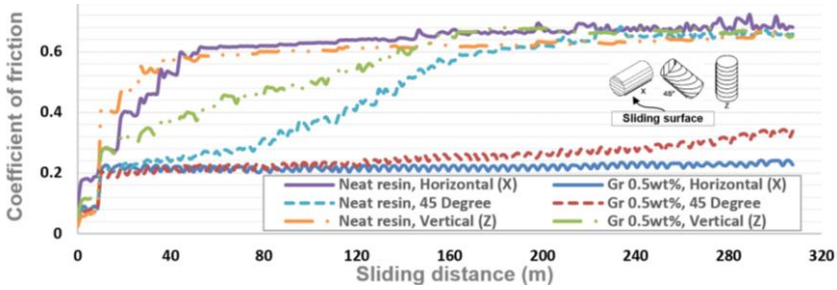

Fig. 5. Friction behaviour of 35 µm layer thickness specimens

The coefficient of friction was reduced tremendously in most of the specimens that contained graphene than in those without it, primarily in the horizontally oriented samples regardless of the layer thickness and print orientation (see Fig. 6a). The values clearly decreased and roughly reached in some cases to half of the corresponding value in the neat resin material chart. This may be because of the effect of graphene as a solid lubricant. However, the results of other speciemens printed with higher graphene ratios (up to 2 wt.%) showed that increasing the percentage of graphene beyond 0.5% by weight did not reduce the coefficient of friction. Hence, for the used graphene/resin composite material in this work, the graphene percentage of 0.5 wt.% was considered the optimum ratio for attaining the best friction behaviour results.

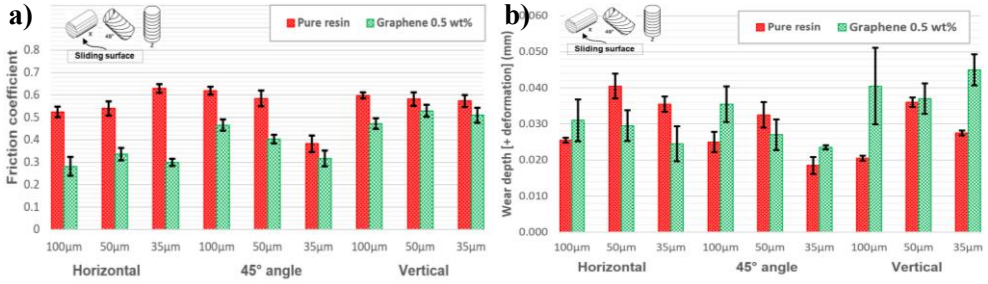

Fig. 6. Comparison of a) friction coefficient, and b) wear depth

A comparison of wear depth for neat resin and graphene (0.5 wt.%)/resin composite specimens under all tested printing settings is shown in Fig. 6b. Concerning the Horizontal build orientation, generally, the graphene/resin composite specimens offered lower wear depth values than the neat resin specimens. This is because of the existence of graphene platelets in the sample's sliding surface which may provide better resistance to the specimen's surface. This can be also connected to the alignment direction of graphene nanoplatelets within the polymer matrix. The arrangement of graphene inside the polymer bulk resembles the isostress (see Fig. 7a) configuration. Hence, the alignment direction tends to have the lower surface area of graphene platelets facing the printing platform top surface.

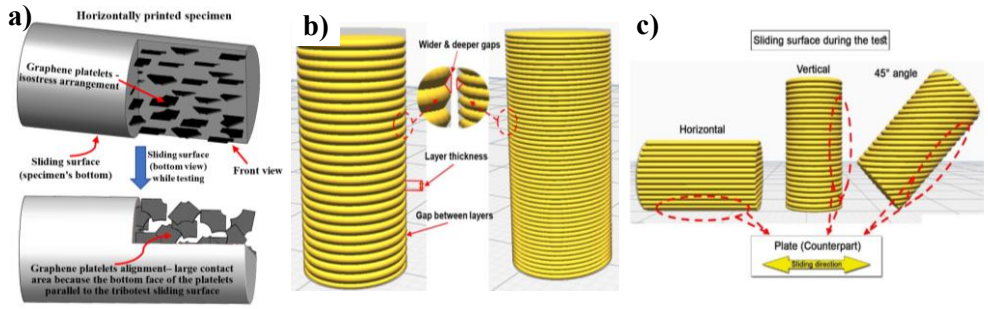

Fig. 7. Schematic of a) graphene platelets alignment, b) gaps among layers for a layer thickness of 100 µm (left) and 35 µm (right), and c) sliding surface roughness

Based on the above, when testing the horizontally printed specimen, the graphene platelets in this print orientation have larger contact area during the tribo-test considering its arrangement direction at the specimen's bottom (Fig. 7a, sliding surface view). This large area helps to enable these platelets to act as a solid lubricant and decrease the wear. On the other hand, the samples' wear depth of graphene/resin composite at 45° angle and Vertical orientations increased compared with that of the neat resin by 98% and 64% at the 100 µm and 50 µm layer thicknesses, respectively. This may be because of the surface roughness of these orientations' specimens, as their sliding surface is rougher than in the Horizontal (see Fig. 7c), which would cause significant wear from

deformation. Accordingly, an elevated wear level was detected in the Vertical surface against the Horizontal.

The impact of increasing the graphene content on the wear depth was examined as well. The results showed that the most favourable wear depth was at graphene percentage of 0.5 wt.%, as increasing the graphene ratio to 1 wt.% or 2 wt.% did not improve the wear attitude.

3.2. Investigation of mechanical characteristics

3.2.1. Tensile of neat PLA material FDM 3D-printed

In terms of the build orientation effect (Fig. 8a), vertically aligned samples (Upright) displayed brittle failure and distinctly inferior tensile strength (only 15.64 MPa) compared with horizontally aligned (Flat) and On-edge samples (averaging less than 61% and 68%, respectively), which both displayed more or less ductile failure. This is due to the orientation of the Upright infill layer perpendicular to the applied load, that in turn, permits individual layers disengaging under the load.

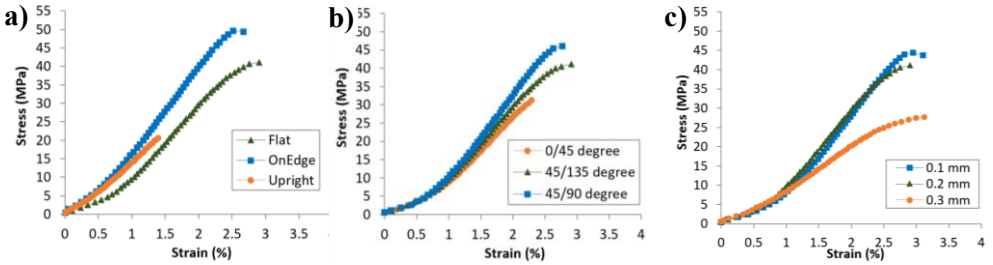

Fig. 8. Stress-strain curves at different a) orientation, b) raster angle, and c) layer thickness

When evaluating the strength of different raster angle specimens (Fig. 8b), the [45/90°] specimens had the highest value (44.97 MPa), while [45/135°] raster direction angle appeared to affect strength as 10.5% weaker. However, [0/45°] demonstrated a lower strength proportion of 30.1% and 21.9% than [45/90°] and [45/135°] test pieces, consecutively. This notable decline can be explained due to the infill raster angle of the [0/45°] sample is perpendicular to the tensile test load, which leads to dismantling the print lines with modest strength and elongation.

Regarding layer thickness impact (Fig. 8c), the highest tensile strength was observed in the lowest layer thickness specimens. This is due to the strength of FDM parts improves with increasing the total number of layers, since the number of layers increases as the layer thickness decreases.

3.2.2. Tensile of bronze/PLA composite FDM 3D-printed

The tensile test results are revealed in Fig. 9a. It can be clearly seen that curves are categorized into three groups in accordance with the tensile properties.

Among the tested specimens, the Flat was the most ductile, whereas the On-edge is the strongest, meanwhile, the Upright was the most brittle. The On-edge specimens obviously could withstand almost double of the stress load that has been applied on the Flat and Upright ones.

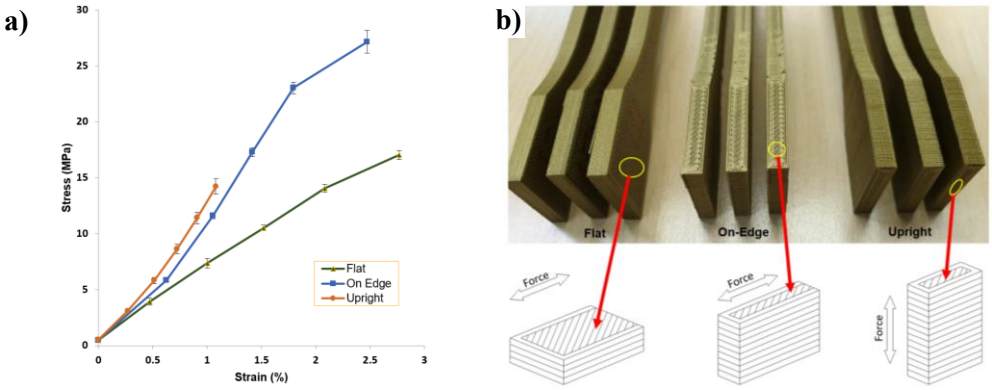

Fig. 9. a) Stress-strain curves, and b) structure of various orientations 3D printing

The structure of the printed tensile test specimens is displayed in Fig. 9b. Every layer contains the contour (shell) and the inner lines. In the case of Flat test pieces, the direction of the layers' contour is parallel with the applied force of the tensile test. As the long inner lines were built at a 45° angle with a moderate number of layers, that increases the possibility of these samples for more elongation (higher strain). The On-edge workpiece has a complicated structure since its cross-section possesses a relatively small size contour with a massive number of layers and short inner lines. This interprets the high strength that these samples offered when pulled during the test. Concerning the Upright samples, the layers are built vertically up to each other and are not interlocked by the printed inner lines but only by the adhesion among layers. Therefore, these specimens are quickly fractured when stretched by the applied force, which makes its attitude brittle.

3.2.3. Tensile of neat resin DLP 3D-printed

The stress-strain curves of the On-edge specimens at each build orientation angle are represented in Fig. 10a and Fig. 10b for samples after and without post-curing process, respectively. According to the results, it can be clearly seen that 0° build orientation angle specimens demonstrate much greater mechanical properties as compared to the 45° and 90° build orientations specimens. This could be explained that the specimens built in 0° orientation angle have a higher number of built layers which are parallel to the direction of applied load during the tensile test, that leads to greater mechanical strength.

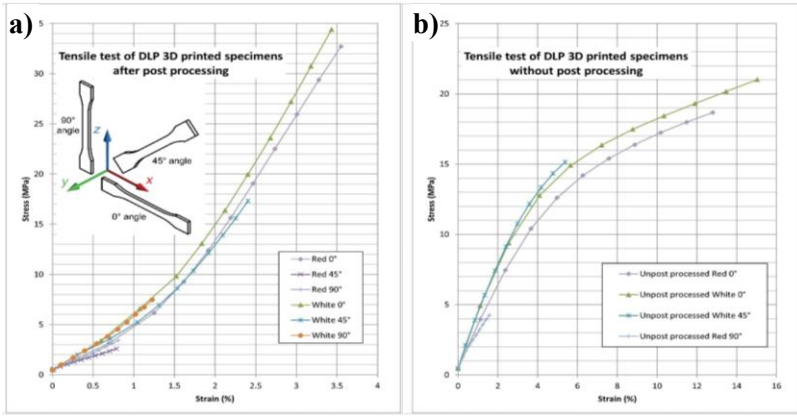

Fig. 10. Stress-strain curves for specimens a) UV post-cured, and b) non-cured

Regarding the impact of post-processing, it is obviously shown that the tensile stress of DLP specimens improved remarkably by the UV post-curing process. In contrast, the value of elongation at the break was significantly decreased for the UV post-cured specimens in front of the non-cured ones.

3.2.4. Tensile of graphene/resin composite DLP 3D-printed

The stress versus strain curves of tensile testing for different layer thickness (35, 50, and 100 µm) specimens are demonstrated in Fig. 11. These curves for the test piece materials of 0 (neat resin), 0.5, and 1 wt.% graphene concentration. In general, the highest tensile strength attitude was observed in the layer thickness of 35 µm. This is because the strength of 3D-printed objects enhances with the increase in the number of the layers, as the lower the layer height the more the number of layers. Therefore, the neat resin specimens reported a reduction of 11.62% and 22.1% in the average values of the tensile stress for 50 and 100 µm layer thickness, consecutively, as compared to the 35 µm.

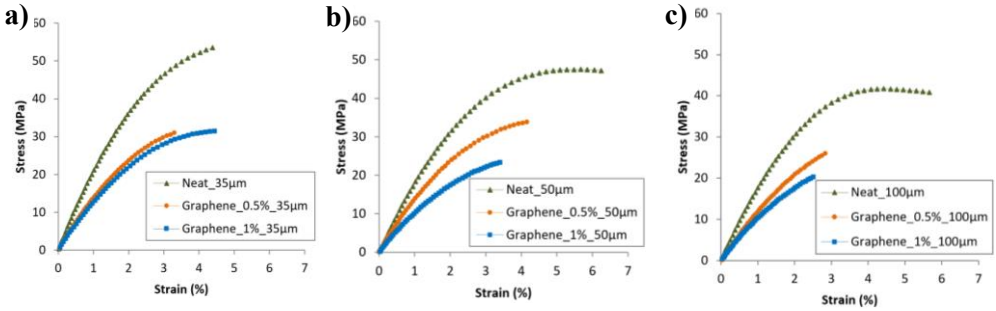

Fig. 11. Stress-strain curves at layer thickness of a) 35 µm, b) 50 µm, and c) 100 µm

Despite the graphene is characterized with high mechanical qualities, however, it can be seen throughout the whole obtained results that the mechanical behaviour was not improved when the graphene nanoplatelets

were integrated. Also, it was noticed that with increasing the graphene concentration further, a much worse mechanical attitude was acquired. This might be attributed to the bubbles created within the matrix bulk during the DLP 3D printing due to the addition of graphene.

3.3. Hardness and surface roughness observation

3.3.1. Hardness and roughness of neat PLA FDM 3D-printed

The PLA specimens were manufactured at three different printing parameters (build orientation, raster angle, and layer thickness) with three levels for each. The hardness measurements were performed at the gripping, curvature, and gauge sections. Three points of measurement were conducted on each section investigated, and the average was calculated. The hardness value ranges in Shore D (77.5 – 78.5), (78 – 80), and (74.5 – 75), for Flat, On-edge, and Upright print orientation, (78.5 – 81), (77.5 – 78.5), and (77.5 – 78.5) for [0/45°], [45/135°], and [45/90°] raster direction angle, and (81), (77.5 – 78.5), and (79.5 – 80.5) for 0.1 mm, 0.2 mm, and 0.3 mm layer thickness specimens, respectively (see all results compared in Fig. 12a).

The results of build orientation specimens show that the On-edge exhibited the highest hardness value. This can be ascribed to the contour (the shell of each layer) of this specimen, as it was in contact with the penetration indenter (test needle). Owing to the fact that the shell is fundamentally much rigid compared to the filling face, the hardness therefore increases. In terms of raster angle specimens, [45/135°] and [45/90°] displayed almost the same values with even similar standard deviation. However, the [0/45°] angle showed slightly higher hardness due to the stability of the short inner lines of [0/45°] pieces. The layer thickness samples revealed the best hardness in the 0.1 mm specimen. This result was expected which can be interpreted due to the presence of fewer voids when the number of layers is more.

The surface roughness measuring test line was carried out within/align-with the sliding area of the tribological test. The measured profiles of specimens examined before and after the tribology test (see Fig. 12b) demonstrate that the Horizontal samples were much smoother than the 45° angle and Vertical ones, where a significant fluctuation (hills and valleys) was noticed, indicating an obvious waviness on these orientations' surfaces. The surface of Horizontal pieces is smoother because the measuring sensor (probe) is aligned with the inner printed lines, and no wrinkles are facing it. In comparison, 45° angle and Vertical specimens revealed a rough surface. This due to the test line is perpendicular to the layers' construction where the probe runs across the valleys and peaks of the entire layers.

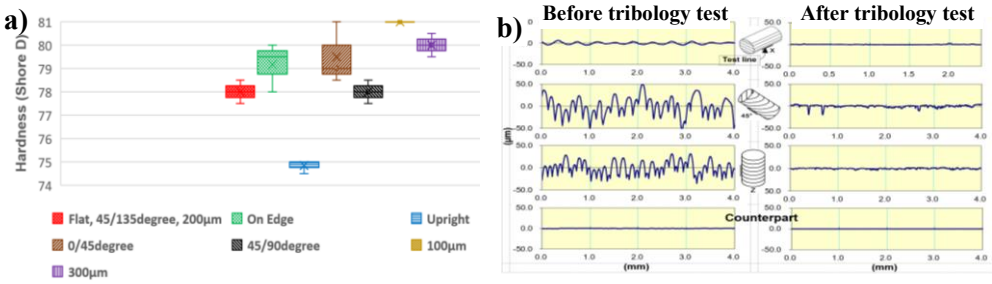

Fig. 12. Results of a) hardness, and b) measured profile in various print orientations

After the tribological tests, the surface roughness measurements were achieved again. The results displayed a significant change in the measured profile in all specimens against the results prior to the test. This evidence the occurrence of wear by removing the facing rough layers during the tribological test.

3.3.2. Hardness and roughness of bronze/PLA FDM 3D-printed

The hardness of three FDM manufactured specimens (one from each print orientation) was estimated using Shore D hardness measurements. The hardness ranges (63 – 67), (70 – 72), and (72.5 – 76) Shore D for Flat, On-edge, and Upright print orientation specimens, respectively, as shown in Fig. 13a. The highest values were reported at the Upright and On-edge samples because the test penetration needle was in contact with the shell of the print, which is harder. While the needle was in contact with the filling face in the Flat test piece. The hardness of the bronze/polymer composite also depends on the incorporated volume percent of polymer particles.

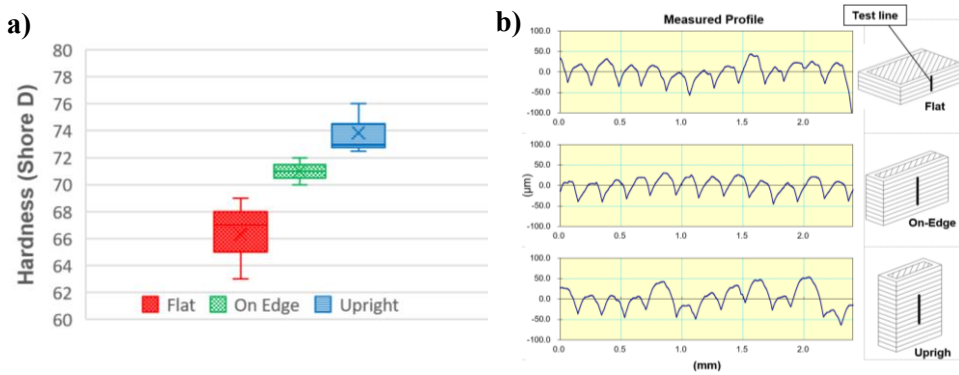

Fig. 13. Results of a) hardness, and b) surface roughness measured profile

The surface roughness measured profile of each print orientation is shown in Fig. 13b. The dark line at the right side of the figure illustrates the path of the measurement where the test was done. In all cases, the measurement track was perpendicular to the layers build direction where the shell can be found. The measured profile showed more regular behaviour at the On-edge sample. This is due to peaks and valleys of the entire layers seem quite uniform and its depth

is insignificant. While Upright specimen reflected the roughest surface since the structure contains non-regulated layers due to the stacking of the printed material.

3.3.3. Hardness and roughness of neat resin DLP 3D-printed

It can be clearly seen in Fig. 14 that the hardness of the post-processed samples is higher. The hardness increased as an obvious consequence of the post-processing. On the contrary, the hardness measurement recorded a decline when the tested specimens were not post-processed.

Fig. 14. Hardness a) after post-processing and b) without post-curing process

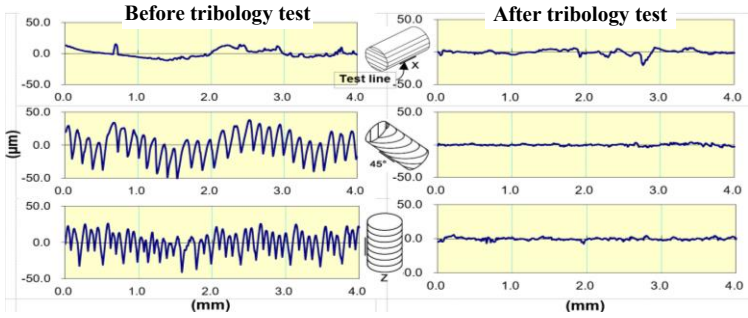

Fig. 15. Surface roughness measured profile before and after tribology tests

Fig. 15 depicts the measured profile for each print orientation before and after tribological tests. Obviously, the smoothest surface could be seen at the X (Horizontal) specimen. This is because the measurement sensor (probe) during the test has passed over the bottom layer (quite smooth) which was in contact with the printing platform. While 45° and Z (Vertical) specimen offered a rougher surface due to the layer structure of the examined surface (like valleys and hills). Certainly, the measured profile of the worn area due to abrading the rough layers during tribology test is smoother than the virgin surface.

3.3.4. Hardness and roughness of graphene/resin DLP 3D-printed

The specimens were made of neat resin material and graphene/resin composite with three various graphene concentrations (0.5, 1, and 2 wt.%). The Shore D hardness value for the neat resin specimen reached nearly 78, while for the specimens of graphene/resin composite the hardness fluctuated around 78.5–

79, 77.5–78, and 79.5–80.5 for graphene content of 0.5, 1, and 2 wt.%, respectively, as displayed in Fig. 16a. It can be seen that the hardness value increased as the graphene ratio increased. The highest value was detected in the specimen of 2 wt.% graphene concentration. The hardness increased as a clear consequence of the existence of graphene, which is much harder than the polymer matrix.

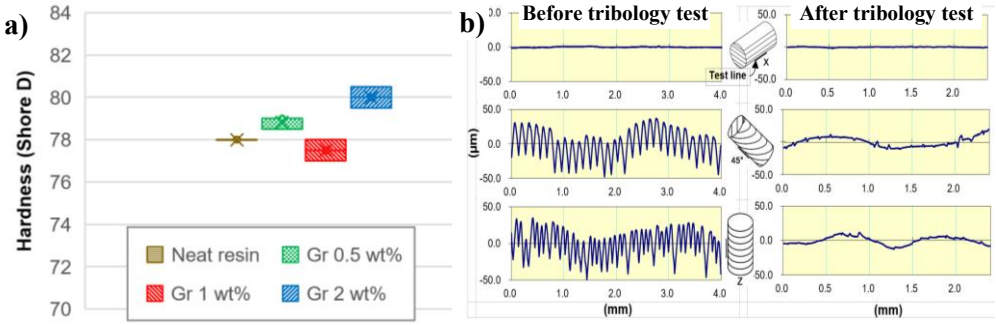

Fig. 16. Results of a) hardness, and b) surface roughness measured profile

The measured profiles (Fig. 16b) showed a tendency similar to the previously examined materials (see Fig. 12b and Fig. 15) regarding the notable smoothness of the Horizontal specimen than other orientations, and polishing the surfaces of all samples after the tribological tests owing to the wear.

In terms of the layer thickness' impact on roughness, the highest increment was observed in the layer thickness of 100 µm. Compared with 50 µm and 35 µm, the surface roughness of 100 µm thickness increased by 54% and 69% for 45° angle specimens and by 52% and 51% for Vertical specimens. The reason for this increase was illustrated in Fig. 7b, as the gaps among the layers of 100 µm are wider and deeper than those at 50 µm and 35 µm.

3.4. Surface structure observation

3.4.1. Surface structure of neat PLA material FDM 3D-printed

Fig. 17a and Fig. 17b displays the optical images of the Horizontal test piece. Obviously, the FDM printing lines were polished after the experiment, indicating material removal due to wear. As mentioned in the surface roughness observations, Horizontal specimens' sliding area has a smoother surface than other test pieces due to its structure. This led to a larger contact area with the mating surface and produced a higher wear rate, which was apparent in the test pieces' burnished surface. The wear track toward the sliding direction can be seen clearly. A lot of molten and then resolidified debris are noticeable as well.

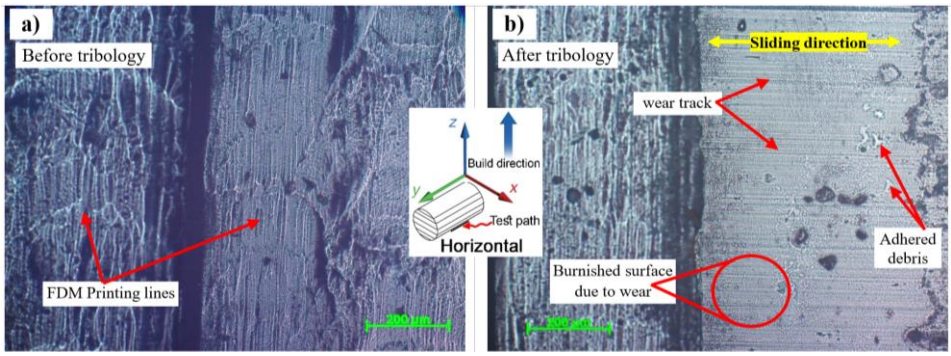

Fig. 17. Surface morphology of Horizontal print orientation specimen before and after test

3.4.2. Surface structure of bronze/PLA composite FDM 3D-printed

Micrographs of the perimeter morphology of some bronze/PLA cylindrical specimens after the tribology test are shown in Fig. 18a and 18b. The existence of an abrasive wear mechanism was confirmed by the microscope images of different print orientations, which showed marks of pitting and grooves. Those asperities contributed to alteration of the surface roughness, which influenced the tribological behaviour. The extent of sliding distance also affects the surface roughness and, implicitly, the wear behaviour. When wear occurs, the surface of the specimen has a higher roughness. Hence, the top layer wears off easily, presenting a higher wear rate. As the sliding distance increase, the high slope of the wear rate decreases. As wear progresses, a glaze forms on the specimen sliding surface, which cause a significant reduction in the rate of wear.

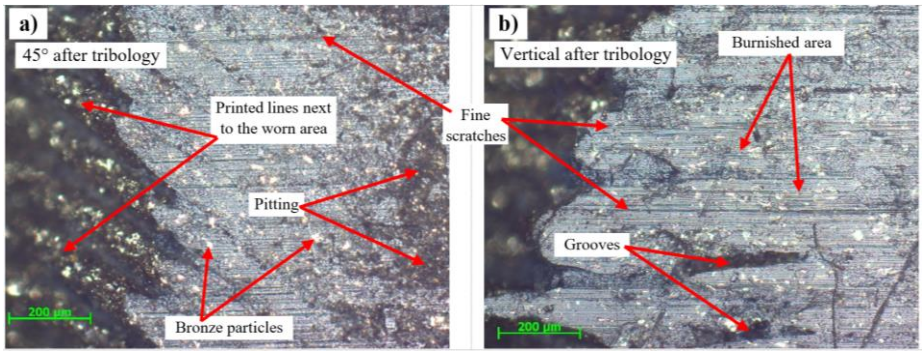

Fig. 18. Surface morphology of bronze/PLA specimens after tribology test

3.4.3. Surface structure of neat resin material DLP 3D-printed

A vertically (Z) printed specimens before and after tribological testing are represented in Fig. 19. Uncured resin particles were manifested at the vertically printed lines before examining the wear. This indicates the insufficient UV curing time during the manufacturing process. Creation of surface asperities and cavities in the sliding surface have been observed

following the tribology test. These asperities (rough surface) contribute to reducing the contact areas. Thus, the friction coefficient augments due to increasing the pressure. This interprets the high values that were reported for the coefficient of friction.

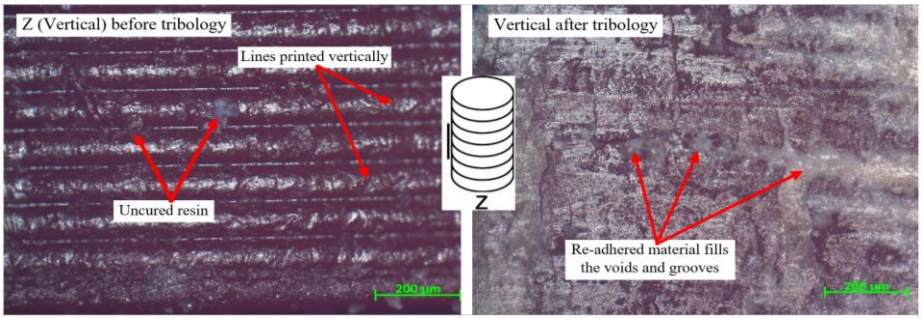

Fig. 19. Microscopic images of a specimen's surface prior and later tribology

3.4.4. SEM of graphene/resin composites DLP 3D-printed

Three different relaxation times after mixing the graphene with resin by vortex mixer shaker were implemented for printing pretest specimens. These times are freshly made (immediately after mixing), after one day, and after one week. The graphene/resin composite used for the microstructure examination is the one with 0.5 wt.% graphene.

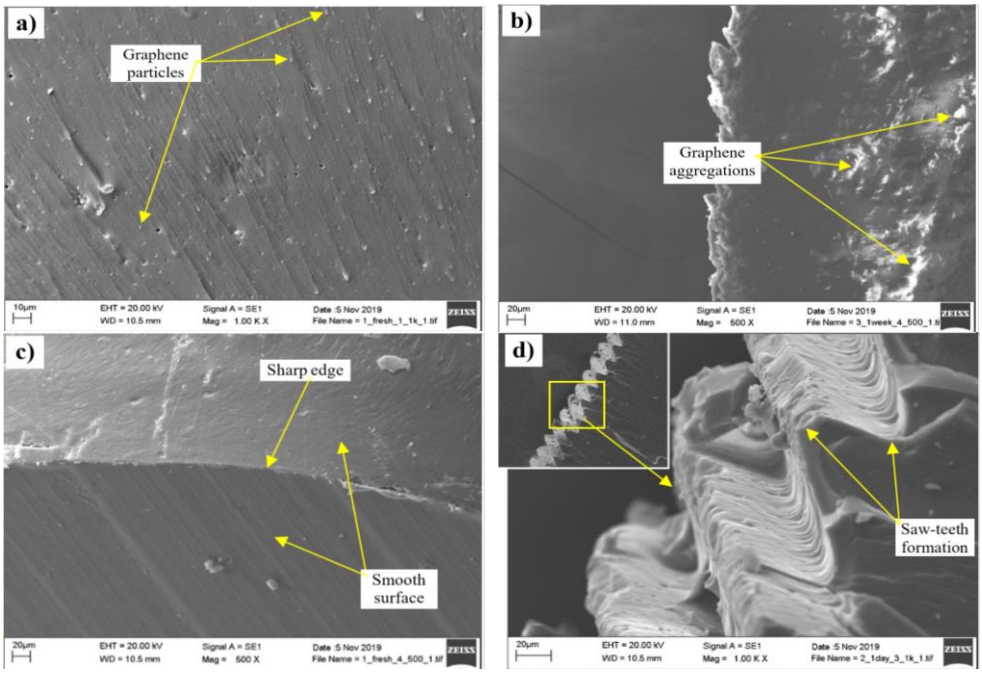

Fig. 20. Microstructure of graphene/resin specimens printed after a) freshly mixing, b) one week of mixing; fracture of c) freshly mixing, and d) one day of mixing

Fig. 20a show that graphene particles were found on the samples (freshly mixed) and successfully incorporated into the printed structure and appear to be distributed evenly throughout the surface. The surface view of the printed sample after one week of mixing clearly depicts the aggregations' formation of precipitated graphene particles (Fig. 20b). This suggests that graphene platelets have lost their uniform distribution over the sample's body structure after one week.

The fracture behaviour of the freshly mixed specimen is depicted in Fig. 20c. While the surfaces in general are almost smooth, sharp edges can be seen in the breakage areas. Fig. 20d highlights the morphology of the fractured cross-section (one-day sample) and shows an interesting phenomenon of the fracture pattern in a saw-teeth form. This may be resulted from the final separation of aggregated graphene platelets.

3.5. Determination of surface energy

The PLA samples' surface was dissolved when introduced to the diiodomethane and cyclohexane. Therefore, it was not possible to determine its surface free energy values by the two-liquid (Fowkes) method. Accordingly, the PLA was only examined by the single-liquid (Eos) method using water. During the measurement, well-examined, constant-volume droplets that did not flow were obtained. The measurement recordings are given in Fig. 21. The calculated surface free energy value is $\gamma = 9.64$ (mN/m).

Fig. 21. Photograph of a water drop residing on FDM 3D-printed PLA surface during the measurement using the Eos method, for three tests at identical conditions

Regarding DLP 3D-printed Resin, the calculated surface free energy value is $\gamma = 41.09$ (mN/m) when determined by single-liquid (water) measurement (Eos model). However, when it was determined by two-liquid (diiodomethane and cyclohexane) measurement (Fowkes method), the calculated surface free energy value is $\gamma = 38.30$ (mN/m).

The measurement results show that DLP 3D-printed resin has a high surface free energy (41.09 mN/m). High surface energy means a stronger tendency to adhesion, and greater friction thus may occur during sliding.

4. NEW SCIENTIFIC RESULTS

The tribological and mechanical characteristics of 3D-printed polymers and polymer composites were comprehensively investigated in this study. The following points are noteworthy to be mentioned:

1. Correlation between the manufacturing process parameters and the tribological properties

I found that the 3D printing parameters (build orientation and layer thickness), strongly influence tribological characteristics in the context of surface waviness/roughness.

Print orientation has an effect on wear based on the surface's macro geometry formed. The Horizontal orientation is smooth compared to other build orientations (e.g., the surface roughness (R_a) of Horizontal is 65–98% lower than the 45° angle and Vertical). Accordingly, I confirmed that if the surface of the specimen is more rough (due to the smaller contact area), the surface layers will wear easily, resulting in a higher abrasion rate (around 32%). Also, I have created a 3D CAD model utilizing the same print orientations examined, focusing on the sliding surfaces' macro geometry. I found that the wear depths of the model's surfaces are in good agreement with the results obtained experimentally.

As the print layer thickness increases, the surface roughness increases, where the rough peaks suffer further and faster wear compared to the smoother surfaces. These findings are supported by my tribological test results, where the wear depth was reduced by 27.2% and 31% for the 50 and 35 μm layer thicknesses, respectively, compared to the 100 μm samples.

2. The impact of composite fillers on the tribological and mechanical characteristics

I have established that the addition of graphene (which can act as a solid lubricant) significantly impacted the coefficient of sliding friction, which was reduced by up to 50% in the graphene-containing samples (mainly in the Horizontal position regardless of layer thickness) compared to the neat resin samples. I found that the optimal graphene volume in the matrix when its concentration does not exceed 0.5 wt.% as it provides better tribology characteristics and also does not reduce the mechanical behaviour.

I observed that graphene resulted in different behaviour in terms of its mechanical properties. Graphene nanoplates did not improve Young's modulus and UTS. Upon further increase of the graphene concentration, worse mechanical properties (almost 24.7%) were obtained due to the increase in porosity. This clearly shows that the preferred tribological characteristics of the graphene/polymer composite plain bearing are coupled with poorer mechanical features.

I investigated composites with high graphene concentrations prepared with an efficient mixing method (lab vortex procedure). I was able to print composites with a graphene ratio of 2 wt.% by the photopolymerization technique. I proved the reliability of the satisfactory mixing method of the uniformly distributed graphene platelets, which was confirmed by the microstructural SEM images. I have shown that the freshly mixed sample is uniformly distributed on graphene plates with a smooth fracture surface. However, the pieces printed after one day or one week of resting showed a saw-teeth shape formation in the cross-section of the fracture, as most of the graphene platelets were detached.

3. The effect of graphene platelets alignment on friction and wear behaviour

I found a correlation between the effect of adjusting graphene platelets and the friction and wear behaviour. The arrangement of graphene in the polymer is similar to the isostress configuration (the lower surface of the graphene platelet faces the upper surface of the printing platform). When testing a horizontally printed specimen, the graphene platelets have a larger contact area during the tribo test, taking into account its orientation at the bottom of the specimen. This large area allows these platelets to act as a solid lubricant and reduce friction and abrasion. As a result, the coefficient of friction has been significantly reduced, and in some cases (especially horizontally) has reached roughly half the value of pure resin material.

I showed that the wear depth of the graphene/resin composite samples increased by 98% and 64%, respectively, at an angle of 45° and a Vertical orientation at a layer thickness of 100 µm and 50 µm, respectively. This is due to the fact that the cross-section of the nano-platelets face the sliding surface due to the arrangement orientation of the graphene platelets, as the samples in the Vertical/45º orientation are placed in a flat (plane) position during the test. This will make the contact area much smaller and increase roughness and wear.

4. The influence of material's colour

I ascertained that the filaments with various colours, due to different additives, reflects an obvious impact on the coefficient of friction of the test pieces. White colour samples gave the highest coefficient of friction while the lowest gave grey. Black specimens reported high wear depth. I stated that this could be related to the characteristics of the black body, where the maximum heat retains in the body of the sample, causing thermal softening and faster melting of the sliding surface layers. I proved this through some heat-conductive tests were carried out on the same examined tribology specimens. The black kept the heat for a longer time, indicating the formation of higher temperatures and therefore determining the tribological behaviour.

5. CONCLUSIONS AND SUGGESTIONS

In this study, the tribological and mechanical behaviour of FDM and DLP 3D printing polymer and polymer composites were reviewed exhaustively. Based on the assessment of the results, the following observations can be drawn:

In the FDM 3D printing:

- The Young's modulus and UTS are maximum at On-edge print orientation due to its robust construction, while elongation at UTS and elongation at break are better at Flat orientation.
- The friction coefficient of 45° angle and Vertical orientation samples decreased at higher load due to the deformation in the contact area caused by the rough surface.
- The occurrence of the stick-slip phenomenon was more likely in the context of sliding under low loads, but wear was diminished.
- The Upright and On-edge samples disclosed a higher hardness, due to the test needle was in contact with the shell which is more solid than the inner print filling.

In the DLP 3D printing

- The highest tensile strength attitude was observed in the lowest layer thickness (35 μm) specimens, due to the increase in the number of layers.
- The UV post-curing process played a significant role in the augmentation of the tensile stress value, but meanwhile diminution the elongation at the break.
- The dynamic coefficient of friction in the 0.5 wt.% graphene specimens disclosed a significant decrease (reached up to 50%) as the graphene acted as a solid lubricant.
- The horizontally printed specimens have offered the smoothest surface as compared to other build orientation samples.

This topic is extremely fertile to be further explored, as quite a lot of aspects are still not covered yet. To highlight some of which, numerous recommendations can be suggested. In the same used cylinder-on-plate tribometer, varying more testing parameters (e.g., sliding speed) should be conducted to investigate its influence, in the context of 3D printing settings, on wear and friction. Also, further studies on the performance of 3D-printed objects under other tribo systems (e.g., pin-on-disk, block-on-ring, etc.) should be carried out. Moreover, much more composite materials (including bio-composites) can be tested as well.

6. SUMMARY

THE EFFECT OF 3D PRINTING STRUCTURES AND SURFACES ON THE TRIBOLOGICAL BEHAVIOR OF POLYMER AND POLYMER COMPOSITES

In summary, the tribological and mechanical behaviour of two 3D printing technologies (FDM and DLP) were studied comprehensively. Various print settings and material colours were used during the specimens' manufacture. The experiments of tribological tests were performed in alternative reciprocating sliding under dry conditions. The effect of 3D printing parameters and additives' existence on the coefficient of friction, wear depth, and specific wear rate were evaluated. The tensile tests were investigated on 3D-printed specimens. SEM and optical microscope were used to study the microstructure and the surface morphology of printed components prior to and after the tribological tests. Hardness and surface roughness of specimens were also tested and analysed for their association with tribological behaviour.

For FDM 3D-printed specimens, the results showed that the white colour samples have offered the highest friction coefficient, whereas the lowest was observed at the grey. The black coloured specimens reported a high wear depth rate. The occurrence of the stick-slip phenomenon was more likely in the context of sliding under low loads. Further, the wear depth reduced with growing the applied load. The friction coefficient of 45° angle and Vertical orientation samples decreased at higher load due to the deformation in the contact area. The Young's modulus and UTS are maximum at On-edge print orientation due to its robust construction, while elongation at UTS and elongation at break are better at Flat orientation. Meanwhile, the Upright sample showed a very fragile behaviour, with extremely rapid fracturing of the printed layers at the break point. The print orientation has the highest contribution parameter which affects mechanical features of the used materials compared to the other examined 3D printing process factors.

For DLP 3D printing, the non-cured specimens demonstrated the highest wear depth and lowest friction coefficient as compared to the cured ones. Based on the SEM images, the freshly mixed sample showed a uniform distribution for graphene platelets with a smooth fracture surface. The graphene percentage of 0.5 wt.% was suggested as the optimum ratio for attaining the best tribological behaviour results in this work, as it decreased the friction coefficient roughly 50%. The highest tensile strength attitude was observed in the lowest layer thickness (35 μm) specimens, due to the increase in the number of layers. A worse mechanical attitude was gained when increasing the graphene concentration, owing to the porosity increase. The horizontally printed specimens have offered the smoothest surface as compared to other build orientation samples. The post-processing has increased the hardness of specimens. Also, the hardness increased with the increase in graphene ratio.

7. MOST IMPORTANT PUBLICATIONS RELATED TO THE THESIS

Refereed papers in foreign languages:

1. **Hanon M. M.**, Zsidai L. (2021): Comprehending the role of process parameters and filament color on the structure and tribological performance of 3D printed PLA. *Journal of Materials Research and Technology, Elsevier.* 15, 647-660. ISSN: 2238-7854, DOI: 10.1016/j.jmrt.2021.08.061, (IF: 5.039*).
2. **Hanon M. M.**, Ghaly A., Zsidai L., Szakál Z., Szabó I., Kátai L. (2021): Investigations of the mechanical properties of DLP 3D printed graphene/resin composites. *Acta Polytechnica Hungarica, Obuda University.* 18 (8), 143–161. ISSN: 1785-8860, DOI: 10.12700/APH.18.8.2021.8.8, (IF: 1.806*).
3. Dobos J., **Hanon M. M.**, Oldal I. (2021): Effect of infill density and pattern on the specific load capacity of FDM 3D-printed PLA multi-layer sandwich. *Journal of Polymer Engineering, De Gruyter.* ISSN: 0334-6447, DOI: 10.1515/polyeng-2021-0223, (IF: 1.367*).
4. **Hanon M. M.**, Marczis R., Zsidai L. (2021): Influence of the 3D Printing Process Settings on Tensile Strength of PLA and HT-PLA. *Periodica Polytechnica Mechanical Engineering, Budapest University of Technology and Economics.* 65 (1), 38–46. ISSN: 1587-379X, DOI: 10.3311/PPme.13683, (Scopus Q2, CiteScore: 2.9*).
5. **Hanon M. M.**, Alshammas Y., Zsidai L. (2020): Effect of print orientation and bronze existence on tribological and mechanical properties of 3D-printed bronze/PLA composite. *The International Journal of Advanced Manufacturing Technology, Springer*. 108: 553–570. ISSN: 0268-3768, DOI: 10.1007/s00170-020-05391-x, (IF: 3.226*).
6. **Hanon M. M.**, Marczis R., Zsidai L. (2020): Impact of 3D printing structure on the tribological properties of polymers. *Industrial Lubrication and Tribology, Emerald*. 72(6): 811–818. ISSN: 0036-8792, DOI: 10.1108/ILT-05-2019-0189, (IF: 1.29*).

International conference proceedings:

7. **Hanon M. M.**, Dobos J., Zsidai L. (2021): The influence of 3D printing process parameters on the mechanical performance of PLA polymer and its correlation with hardness. *DET 2020, Budapest, Hungary*, October 11–13, 2021. Published in: *Procedia Manufacturing, Elsevier.* 54, 244-249. ISSN: 2351-9789, DOI: 10.1016/j.promfg.2021.07.038, (Scopus Q2, CiteScore: 2.3*).